SAR TOMOGRAPHY USING STARING AND HIGH-RESOLUTION SPOTLIGHT DATA FROM THE TANDEM-X PURSUIT MONOSTATIC MODE

Nan Ge [(1)], Xiao Xiang Zhu [(1,2)]

(1) Remote Sensing Technology Institute (IMF), German Aerospace Center (DLR), Oberpfaffenhofen, D-82234 Wessling, Germany (Email: Nan.Ge@dlr.de)
(2) Helmholtz Young Investigators Group: SiPEO, Chair of Remote Sensing Technology, Technische Universität München

1. INTRODUCTION

Synthetic aperture radar (SAR) tomography has been intensively used in urban scenarios to reconstruct the elevation position of each coherent scatterer overlaid within a 2-dimensional focused azimuth-range pixel [1] [2]. For this purpose, observations sampled at different spatial frequencies w.r.t. a reference 'master' scene are needed. Modern algorithms, e.g., SL1MMER proposed by Zhu and Bamler (2010), have been developed to achieve both robustness and super-resolution.

Due to the intrinsic highly heterogeneous nature of urban areas with buildings and other infrastructures, SAR imaging mode with the highest resolution possible is usually favored. This insures a small number of scatterers inside each resolution cell and thus increases the probability of successful recovery. However, data takes over time seem to become obsolete, as older satellites are replaced by their successors which are equipped with upgraded sensors. Besides, new methodologies emerge which contribute to draining more performance out of available hardware. The former could be that the German satellite TerraSAR-X retires and hands its job over to the foreseen Next Generation TerraSAR-X HD, which will possibly be characterized by larger range bandwidth, while steering the radar beam more sharply to synthesize a larger aperture could be an example for the latter. Anyway, SAR data with the same resolution will be discontinued, as long as better resolution is desired. Naturally, the same problem could also arise purely due to the change of public interest within the life span of a satellite.

In this abstract, we propose a new method to jointly carry out tomographic processing on SAR data from the same pipeline but with different resolutions. The data set used in this study will be described in Section 2. Section 3 is dedicated to the demonstration of the mathematical model. An outlook will be given in Section 4.

2. DATA SET

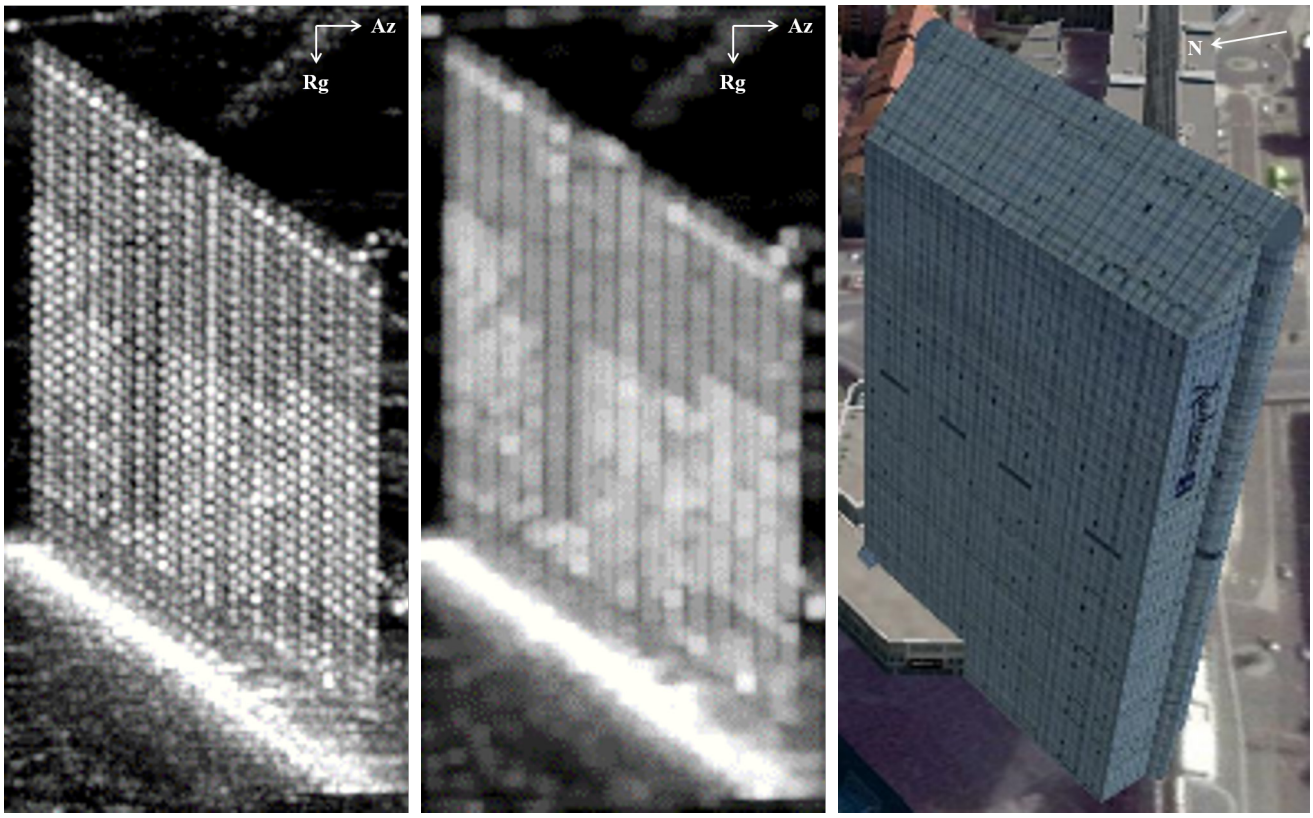

(a) (b) (c)

Figure 1. Building of interest: (a) ST and (b) simulated HS intensity image in [dB]; (c) 3-D photorealistic building model from © Google Earth.

From November 2014 till February 2015, the twin satellites TerraSAR-X and TanDEM-X will operate independently with an along-track distance of approximately 76 km within the first part of the Science Phase [4]. The short revisit time interval between two passes on a single day results in very similar backscattering characteristics and path delay effects. Therefore, pursuit monostatic interferograms from this formation are unlikely to be affected by atmospheric phase screen or motion. We plan to utilize both staring (ST) and high-resolution spotlight (HS) data acquired during this time period with an alternating rhythm.

Fig. 1a illustrates the mean intensity image of a building in ST mode, where each pixel is of approximately the size 0.23m×0.59m (azimuth by range). A corresponding HS intensity image is simulated and shown in Fig. 1b, where the bright scatterers are smeared out. Note that the square pixel is indeed a tall rectangle in reality. This implies that the HS image would still look sharp if downsampled (here oversampled for the sake of comparison with ST). Nevertheless the ST image contains many more details, despite the large sharp angle (roughly 60°, not to scale in Fig. 1a/b) between the building façade and azimuth direction. A 3-dimensional (3-D) building model is given in Fig. 1c as reference.

3. JOINT PROCESSING MODEL

In this section, we develop a generic model to perform tomographic processing on datasets with different resolutions.

As illustrated in Fig. 2, we assume that one low-resolution (LR) pixel L could be represented by J high-resolution (HR) pixels $H_i \forall i = \{1, \cdots, J\}$.

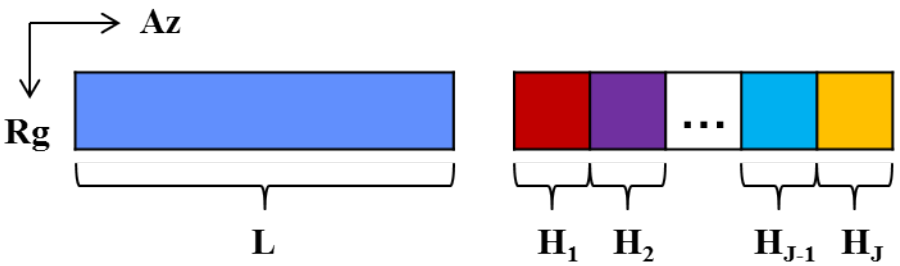

Figure 2. Illustration of an LR pixel L represented by J HR pixels H_i.

For the LR pixel L, we have

$$\mathbf{g}_L = \mathbf{R}_L \, \boldsymbol{\gamma}_L + \boldsymbol{\varepsilon}_L, \tag{1}$$

where $\mathbf{g}_L \in \mathbb{C}^{N_L \times 1}$ is the observation vector sampled at N_L spatial frequencies, $\mathbf{R}_L \in \mathbb{C}^{N_L \times L}$ denotes an overcomplete Fourier matrix with L discretizations on the elevation axis, $\boldsymbol{\gamma}_L \in \mathbb{C}^{L \times 1}$ is the reflectivity vector at those corresponding elevation positions, and $\boldsymbol{\varepsilon}_L \in \mathbb{C}^{N_L \times 1}$ stands for additive Gaussian random noise. Similarly, we have for the HR pixels

$$\begin{aligned} \mathbf{g}_{H_1} &= \mathbf{R}_H \, \boldsymbol{\gamma}_{H_1} + \boldsymbol{\varepsilon}_{H_1}, \\ &\vdots \\ \mathbf{g}_{H_J} &= \mathbf{R}_H \, \boldsymbol{\gamma}_{H_J} + \boldsymbol{\varepsilon}_{H_J}, \end{aligned} \tag{2}$$

where $\mathbf{g}_{H_i}, \boldsymbol{\varepsilon}_{H_i} \in \mathbb{C}^{N_H \times 1}$, $\mathbf{R}_H \in \mathbb{C}^{N_H \times L}$ and $\boldsymbol{\gamma}_{H_i} \in \mathbb{C}^{L \times 1} \;\; \forall i = \{1, \cdots, J\}$.

Let

$$\boldsymbol{\gamma}_L \coloneqq \boldsymbol{\Gamma}_H \boldsymbol{\alpha}, \tag{3}$$

where $\boldsymbol{\Gamma}_H = \left[\boldsymbol{\gamma}_{H_1}, \cdots, \boldsymbol{\gamma}_{H_J} \right]$ and $\boldsymbol{\alpha} = \left[\alpha_1, \cdots, \alpha_J \right]^{\mathrm{T}}$ is a kernel relating HR pixels to LR pixel. By inserting Eq. (3) into (1), we obtain

$$\mathbf{g}_L = \mathbf{R}_L \, \mathbf{\Gamma}_H \boldsymbol{\alpha} + \boldsymbol{\varepsilon}_L = \sum_{i=1}^{J} \alpha_i \mathbf{R}_L \boldsymbol{\gamma}_{H_i} + \boldsymbol{\varepsilon}_L. \tag{4}$$

Combining Eq. (2) and (4), we get

$$\begin{bmatrix} \mathbf{g}_L \\ \mathbf{g}_{H_1} \\ \vdots \\ \mathbf{g}_{H_J} \end{bmatrix} = \begin{bmatrix} \alpha_1 \mathbf{R}_L & \cdots & \alpha_J \mathbf{R}_L \\ \mathbf{R}_H & 0 & 0 \\ \vdots & \ddots & \vdots \\ 0 & 0 & \mathbf{R}_H \end{bmatrix} \begin{bmatrix} \boldsymbol{\gamma}_{H_1} \\ \vdots \\ \boldsymbol{\gamma}_{H_J} \end{bmatrix} + \begin{bmatrix} \boldsymbol{\varepsilon}_L \\ \boldsymbol{\varepsilon}_{H_1} \\ \vdots \\ \boldsymbol{\varepsilon}_{H_J} \end{bmatrix}, \tag{5}$$

which can be re-written as

$$\mathbf{g} = \mathbf{R} \, \boldsymbol{\gamma} + \boldsymbol{\varepsilon}, \tag{6}$$

where $\mathbf{g}, \boldsymbol{\varepsilon} \in \mathbb{C}^{(N_L + J \cdot N_H) \times 1}$, $\mathbf{R}_L \in \mathbb{C}^{(N_L + J \cdot N_H) \times (J \cdot L)}$ and $\boldsymbol{\gamma}_L \in \mathbb{C}^{(J \cdot L) \times 1}$.

Eq. 6 is a typical sparse reconstruction problem and thus could be solved by, e.g., the SL1MMER method with some minor modifications.

4. OUTLOOK

In this abstract, we have explained our motivation in the first place, followed by showcasing a comparison of typical ST and HS images in urban areas. We then demonstrated our method to jointly process SAR data at different resolutions. Our results will be presented in the full paper.

[1] X. Zhu, R. Bamler, "Very high resolution spaceborne SAR tomography in urban environment", *IEEE Trans. Geosci. Remote Sens.*, vol. 48, no. 12, pp. 4296–4308, 2010.

[2] D. Reale , G. Fornaro, A. Pauciull, X. Zhu, R. Bamler, "Tomographic Imaging and Monitoring of Buildings with Very High Resolution SAR Data", *IEEE Geosci. Remote Sens. Letters*, vol. 8, no. 4, pp. 661–665, 2011.

[3] X. Zhu, R. Bamler, "Tomographic SAR inversion by L1 norm regularization – The compressive sensing approach," *IEEE Trans. Geosci. Remote Sens.*, vol. 48, no. 10, pp. 3839–3846, 2010.

[4] TanDEM-X Ground Segment, "Announcement of Opportunity: TanDEM-X Science Phase," Doc. TD-PD-PL-0032, Issue 1.0, 2014.05.19.